Tritium calibration of the LUX detector

D.S. Akerib,[1] H.M. Araújo,[2] X. Bai,[3] A.J. Bailey,[2] J. Balajthy,[4] E. Bernard,[5] A. Bernstein,[6] A. Bradley,[1] D. Byram,[7] S.B. Cahn,[5] M.C. Carmona-Benitez,[8] C. Chan,[9] J.J. Chapman,[9] A.A. Chiller,[7] C. Chiller,[7] T. Coffey,[1] A. Currie,[2] L. de Viveiros,[10] A. Dobi,[4] J. Dobson,[11] E. Druszkiewicz,[12] B. Edwards,[5] C.H. Faham,[13] S. Fiorucci,[9] C. Flores,[14] R.J. Gaitskell,[9] V.M. Gehman,[13] C. Ghag,[15] K.R. Gibson,[1] M.G.D. Gilchriese,[13] C. Hall,[4] S.A. Hertel,[5] M. Horn,[5] D.Q. Huang,[9] M. Ihm,[16] R.G. Jacobsen,[16] K. Kazkaz,[6] R. Knoche,[4] N.A. Larsen,[5] C. Lee,[1] A. Lindote,[10] M.I. Lopes,[10] D.C. Malling,[9] R. Mannino,[17] D.N. McKinsey,[5] D.-M. Mei,[7] J. Mock,[14] M. Moongweluwan,[12] J. Morad,[14] A.St.J. Murphy,[11] C. Nehrkorn,[8] H. Nelson,[8] F. Neves,[10] R.A. Ott,[14] M. Pangilinan,[9] P.D. Parker,[5] E.K. Pease,[5] K. Pech,[1] P. Phelps,[1] L. Reichhart,[15] T. Shutt,[1] C. Silva,[10] V.N. Solovov,[10] P. Sorensen,[6] K. O'Sullivan,[5] T.J. Sumner,[2] M. Szydagis,[14] D. Taylor,[18] B. Tennyson,[5] D.R. Tiedt,[3] M. Tripathi,[14] S. Uvarov,[14] J.R. Verbus,[9] N. Walsh,[14] R. Webb,[17] J.T. White,[17] M.S. Witherell,[8] F.L.H. Wolfs,[12] M. Woods,[14] and C. Zhang[7]

[1] *Case Western Reserve University, Dept. of Physics, 10900 Euclid Ave, Cleveland OH 44106, USA*
[2] *Imperial College London, High Energy Physics, Blackett Laboratory, London SW7 2BZ, UK*
[3] *South Dakota School of Mines and Technology, 501 East St Joseph St., Rapid City SD 57701, USA*
[4] *University of Maryland, Dept. of Physics, College Park MD 20742, USA*
[5] *Yale University, Dept. of Physics, 217 Prospect St., New Haven CT 06511, USA*
[6] *Lawrence Livermore National Laboratory, 7000 East Ave., Livermore CA 94551, USA*
[7] *University of South Dakota, Dept. of Physics, 414E Clark St., Vermillion SD 57069, USA*
[8] *University of California Santa Barbara, Dept. of Physics, Santa Barbara, CA, USA*
[9] *Brown University, Dept. of Physics, 182 Hope St., Providence RI 02912, USA*
[10] *LIP-Coimbra, Department of Physics, University of Coimbra, Rua Larga, 3004-516 Coimbra, Portugal*
[11] *SUPA, School of Physics and Astronomy, University of Edinburgh, Edinburgh, EH9 3JZ, UK*
[12] *University of Rochester, Dept. of Physics and Astronomy, Rochester NY 14627, USA*
[13] *Lawrence Berkeley National Laboratory, 1 Cyclotron Rd., Berkeley, CA 94720, USA*
[14] *University of California Davis, Dept. of Physics, One Shields Ave., Davis CA 95616, USA*
[15] *Department of Physics and Astronomy, University College London, Gower Street, London WC1E 6BT, UK*
[16] *University of California Berkeley, Department of Physics, Berkeley, CA 94720, USA*
[17] *Texas A & M University, Dept. of Physics, College Station TX 77843, USA*
[18] *South Dakota Science and Technology Authority, Sanford Underground Research Facility, Lead, SD 57754, USA*

We describe the development, deployment, and exploitation of a tritium calibration source for the LUX dark matter experiment. The source is useful for calibrating the electron recoil backgrounds over the full volume of the detector, and for characterizing the behavior of the LUX TPC. We report on the LUX electron recoil discrimination factor, the detector threshold, and on the detector physics of liquid xenon at the LUX electric field value of 181 V/cm.

I. Introduction

LUX is a large dual-phase liquid xenon (LXe) time projection chamber (TPC) located at the 4850' level of the Sanford Underground Research Facility (SURF) in Lead, South Dakota. LUX searches for WIMP dark matter interactions by detecting scintillation (S1) and charge signals (S2) from particle interactions in the LXe. Electron-recoil (ER) and nuclear-recoil (NR) events are distinguished by the ratio of the charge and light signals (S2/S1). Results from the first LUX science run (Run 3) were first reported in Ref. [**?**]. An improved analysis of the Run 3 data is reported in Ref. [**?**].

In the WIMP region of interest (∼1 - 8 keVee), LUX rejects external gamma backgrounds primarily through self-shielding, achieving an event rate of 3.6 mDRU[**?**] between 0.9 and 5.3 keVee in the 118 kg fiducial volume. The LUX TPC reconstructs the three coordinates of the event vertex with a spatial precision of about 1 cm, allowing events near the edge of the detector to be rejected. This effect is substantial in LUX because of the large active mass (270 kg) and favorable aspect ratio (50 cm diameter

and 60 cm height).

To calibrate the ER response of LUX we rely primarily on internal beta sources that can be dissolved in the LXe. External gamma sources, such as ^{137}Cs or ^{228}Th , are unable to produce a useful rate of single-scatter calibration events in the fiducial volume at low energy due to the self-shielding effect. Two internal calibration sources, ^{83m}Kr [**?** **?**] and tritium (^{3}H), have been deployed in LUX, allowing the ER response of the detector to be studied with a large sample of spatially uniform events.

In this article we report results from the calibration of LUX with the tritium source. Tritium is a single-beta emitter with a Q value of 18.6 keVee [**?**]. Are these statements true? Its mean energy is 5.6 keVee [**?**] with a broad peak at 3.0 keVee. 75% of its beta decays are below 8 keVee [**?**]. These characteristics make it an ideal source for studying the ER response of LUX in the dark matter energy range. However, tritium is long-lived, with a half-life of 12.3 years[**?**], so it must be removed by purification. In addition, the tritium must be introduced into the detector in a manner which will not impair the charge or light collection properties of the detector.

We use tritiated methane (CH_3T) as the host molecule to deliver tritium activity into LUX. CH_3T has several advantageous properties compared to molecular tritium (T_2). First, it does not adsorb onto surfaces like the T_2 molecule, and it does not interfere with charge transport in liquid xenon. Secondly, diffusion of tritium activity into the plastic detector parts is an important concern, since such activity may later contaminate the LXe during the WIMP search data runs. This risk is mitigated by CH_3T compared to T_2 due to its larger molecular size and lower diffusion constant and solubility. We ultimately performed a series of experiments with a bench-top LXe detector and samples of the LUX plastics to demonstrate that the injection and removal could be done successfully. These experiments are described in the appendix.

An initial tritium dataset of $\sim$ 7,000 fiducial events was obtained by LUX in August of 2013, and the results were reported in Ref. [**?**]. Subsequently, in December 2013, we injected additional activity with a higher rate and obtained a fiducial tritium dataset of over 150,000 events. This dataset is used to calibrate the LUX ER band in Ref. [**?**]. Except where otherwise noted, in this article we report results from the larger December 2013 dataset.

II. Injection and removal of tritiated methane

Two tritiated methane sources with total activities of 3 Bq and 200 Bq were prepared for use in LUX. Each source is contained in a 2.25 liter stainless steel bottle and is mixed with 2 atmospheres of LUX-quality purified xenon. The xenon acts as a carrier gas to extract the source from the bottle. The tritiated methane was synthesized for LUX by Moravek Biochemical [**?**] at a specific activity of 5 milliCurie per millimol.

The injection system is shown in Fig. 1. A fraction of the source bottle activity may be extracted allowing the carrier gas to expand into one or more expansion volumes consisting of various sections of evacuated tubing. The amount of extracted activity is controlled by selecting an expansion volume of appropriate size. A methane purifier (SAES model MC1-905F) located between the source bottle and the expansion volume ensures that only methane and noble gases are allowed to enter the system. The extracted activity is then injected into the TPC by diverting a small portion of the LUX xenon gas flow through the expansion volumes.

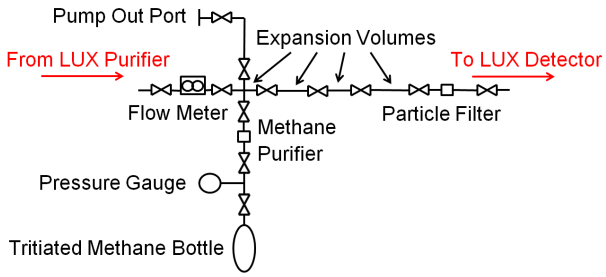

FIG. 1: Plumbing diagram of the tritium injection system for LUX. Tritium is injected downstream of the LUX xenon purifier so that it passes through the detector once prior to being removed. Red arrows indicate the direction of flow.

The tritiated methane appears in the TPC soon after the injection is performed and is removed via the normal action of the LUX xenon purification system, which operates without interruption during the entire procedure. Its centerpiece is a hot zirconium getter (SAES model PS4-MT15-R1) which acts upon gaseous xenon and removes all non-noble species including methane. The xenon gas flow is driven by a diaphragm pump and is facilitated by an efficient two-phase heat exchanger to effect the liquid-

gas phase change [**?**]. The xenon flows in a continuous and perpetual circuit between the TPC and the getter at a rate of 25 SLPM.

Prior to the first injection of tritium activity, we first confirmed that the LUX getter unit was capable of efficient methane removal by injecting ∼1 ppm (part-per-million) of un-tritiated methane (CH_4) into LUX. As shown in Fig. 2, the CH_4 concentration in the gas was observed over the next several days using a mass spectrometer. The natural methane concentration was observed to decrease exponentially with a time constant of 5.9 ±0.07 hours. The one-pass efficiency of the getter for methane was measured to be 97% under the LUX flow and temperature conditions by sampling the gas before and after the getter.

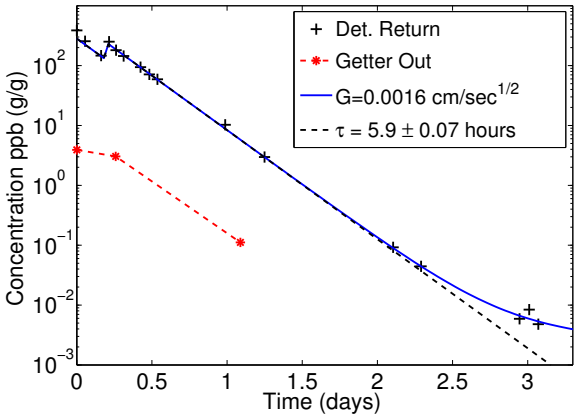

FIG. 2: Removal of natural methane observed by the integrated xenon sampling system prior to the tritiated methane injections. The red points indicate measurements at the getter outlet, we find a 97% one pass removal efficiency at a flow rate of 25 SLPM. The blue curve shows the improved upper limit on the effect of outgassing from the plastics. The black dashed lines shows the exponential fit to the natural methane removal from the xenon with a time constant of 5.9 ±0.07 hours. 5×10^{-3} ppb (g/g) is the limit of detection for methane.

On August 8, 2013, an initial injection of 20 mBq of tritiated methane was performed, followed five days later by an injection of 800 mBq. The count rate of fiducial single-scatter events with S1 less than 150 phe during this time period is shown as a function of time in Fig. 3. The tritium activity is clearly observed. For both injections the activity was removed with a six-hour exponential time constant similar to that observed in the CH_4 injection. It is interesting that the purification time constant is considerably shorter than the naive volume turn-over time of LUX (about 41 hours for 370 kg of xenon at a gas flow rate of 25 SLPM). The origin of short purification time remains under investigation.

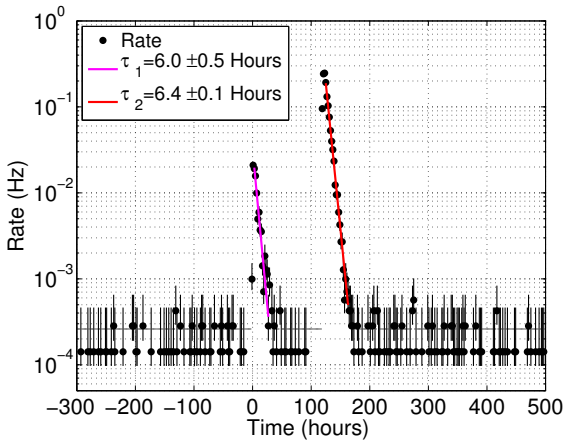

FIG. 3: Left: Rate of single scatter events with S1 below 150 Phe in the fiducial volume during the August 2013 tritium injections. 150 Phe in S1 is about 18.6 keVee, the endpoint of the tritium beta spectrum. The magenta and red curves are exponential fits to the activity vs time.

The location of a the tritium events from the first injection is shown in Fig. 4. As expected the events are uniform within the detector volume.

III. Results

In December of 2013 a total of 10 Bq of tritiated methane was injected into LUX and removed. A total 325,000 events were observed in the active volume of LUX. 140,000 events were collected in the fiducial volume at the nominal LUX electric field of 170 V/cm, while 4,500 fiducial events were collected in a special run at a reduced field of 100 V/cm. The S1 and S2 signals are corrected for spatial effects such as the light collection efficiency and the free electron lifetime with $^{8}3m$Kr data as described in [**?**].

We interpret the data in terms of the combined energy model [**?**], where the total energy of an event is directly

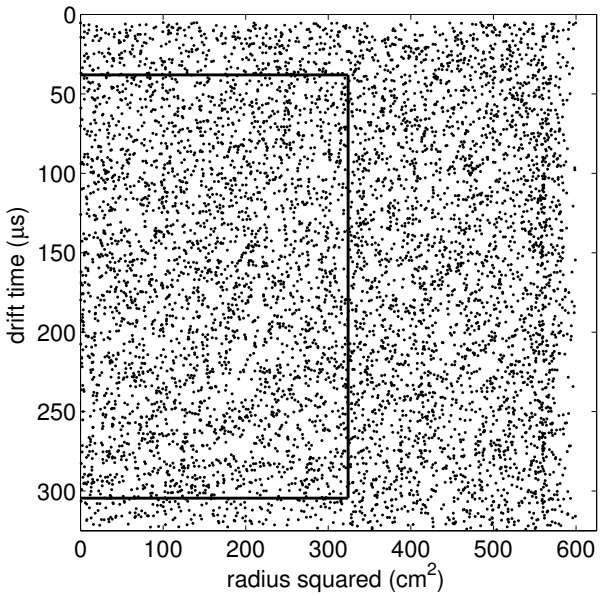

FIG. 4: The location of events in drift time vs. detector radius squared for the first tritium injection. The drift time is a proxy for the z coordinate of the event. The solid black line represents the fiducial volume used in [**?**].

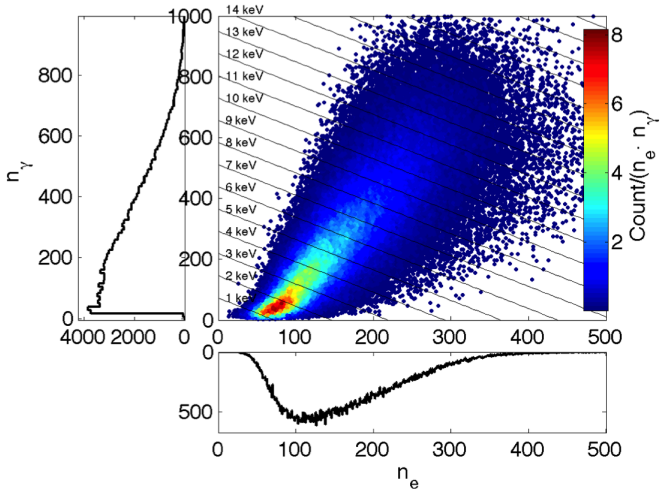

FIG. 5: Scatter plot of n_e vs n_γ for 115,000 fiducial tritium events at 170 V/cm. Lines of constant energy are indicated assuming a W value of 13.7 eV/quanta. The data is projected into n_e and n_γ histograms on each axis.

proportional to the number of quanta produced (electrons pus scintillation photons):

$$E_{total} = W \cdot (n_\gamma + n_e)$$

We use a W value of 13.7 eV/quanta [**?**]. In LUX n_γ and n_e are proportional to the S1 and S2 signals, with gain factors g_1 and g_2:

$$E_{total} = W \cdot (\frac{S1}{g_1} + \frac{S2}{g_2})$$

where S1 and S2 have units of phe and g_1 and g_2 have units of phe per quanta. g_1 may be interpreted as the light collection efficiency times the average quantum efficiency of the PMT arrays, while g_2 is the electron extraction efficiency at the liquid-gas surface times the secondary scintillation gain factor and the PTM quantum efficiency. g_1 and g_2 are measured with line source data in LUX as described in Ref. [**?** **?**]. We find values of $g_1 = 0.115 \pm 0.003$and $g_2 = 5.39 \pm 0.522$.

A scatter plot of n_e vs n_γ for the tritium data at 170 V/cm is shown in Fig. 5, along with the projected histograms on each axis. The tritium energy spectrum, obtained by projecting the data along the lines of constant energy, is shown in Fig. 6. The data is compared to several models: a pure tritium spectrum, with no detector effects; a spectrum simulated with LUXsim, and a tritium spectrum with a simple energy smearing factor of $\sigma_E = XXXX$ applied. The ratio of the data to the smeared tritium spectrum is shown in Fig. 7, along with a fit to an error function. The ratio indicates that the data is well modeled by the smeared tritium spectrum, and the effective 50% energy threshold is found to be 1.04 ± 0.016 keV.

The comparison also illustrates the usefulness of the combined energy model. Compared to the raw charge and light spectra shown projected on the axes in Fig. 5, the combined energy reproduces the tritium spectrum with much greater fidelity.

The mean light yield and charge yield of ER events in LUX are obtained by dividing the mean light and charge signals by the combined energy in each energy bin. The result is shown for 170 V/cm in Fig. 8. For these plots a small correction has been applied to the data to account for smearing of tritium events across energy bins due to

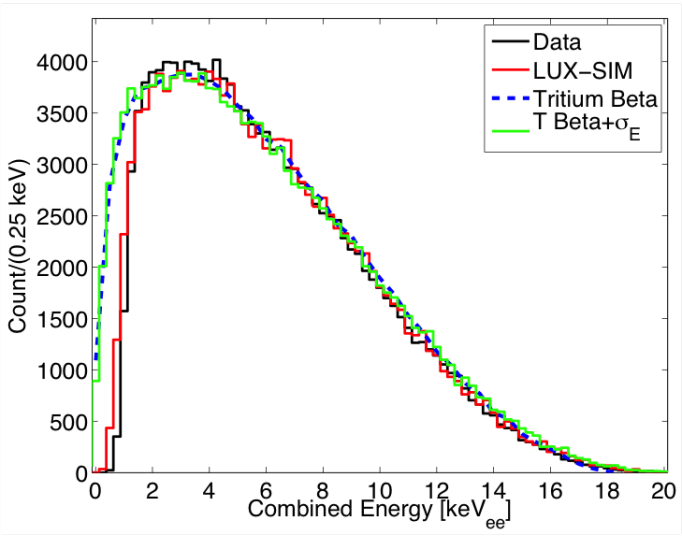

FIG. 6: The tritium energy spectrum measured by LUX with the combined energy model (black) compared to several theory models: a pure tritium spectrum (dashed blue), LUXsim (red) and a tritium spectrum with a simple energy smearing of $\sigma_E = XXXX$ applied.

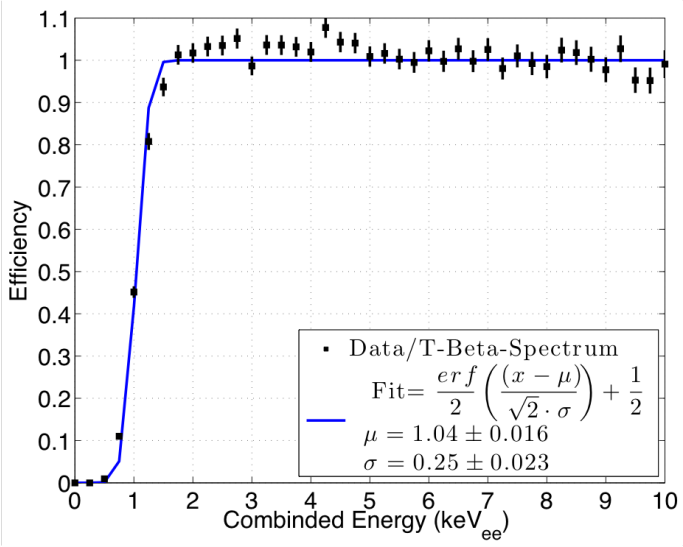

FIG. 7: ER threshold measured by comparing the measured energy spectrum to the smeared tritium spectrum. A fit to an error function is shown.

the detector's resolution [**?**].

As shown in Fig. 8, the light yield is observed to drop rapidly between 1 and 6 keV, and then become mostly energy independent over the remainder of the tritium spectrum. The charge yield exhibits the reverse behavior, as expected from the combined energy model. These effects can also be illustrated by plotting the total number of quanta as a function of energy, as shown in Fig. 9 for tritium events between 1 and 8 keV. Also shown in Fig. 9 are the total number of quanta assuming a W value of 13.7 eV/quanta (black), and the primary number of ions (violet) and excitons (cyan) prior to recombination assuming an initial exciton-to-ion ratio of 0.2 [**?**]. In a model where the number of observed electrons differs from the number of primary ions due solely to recombination, we can interpret the charge yield data as a measure the recombination fraction at each energy. Accordingly,

$$r = \frac{\frac{n_\gamma}{n_e} - \alpha}{\frac{n_\gamma}{n_e} + 1}$$

where r is the recombination fraction and α is the assumed value of the primary exciton-to-ion ratio. Taking $\alpha = 0.2$, we find the recombination fraction as a function of energy as shown in Fig. 10. Here the falling charge yield and rising light yield between 1 and 6 keV is interpreted as a rapid rise in the recombination fraction.

We obtain the LUX ER band by plotting $\log_{10}$(S2/S1) vs S1 as shown in Fig. 11. Also shown is the LUX NR band determined with NEST v0.98 (2013) [**?**] and validated with AmBe and ^{252}Cf neutron sources and DD neutron generator data. The ER band has a characteristic rise at low S1 which reflects the increasing charge yield and decreasing light yield below 4 keVee, as seen in Fig. **??**. The leakage fraction (f), defined as the fraction of ER events that fall below the mean of the NR band, is shown in Fig. 12 as a function of S1. The recoil discrimination ($1 - f$) has an average value of 99.58% for events with S1 between 1 and 30 phe.

Figure 14 shows the reconstructed energy spectrum for those tritium events in the fiducial volume of the detector (black) along with the tritium spectrum from NEST modeling (blue) and an ideal tritium spectrum (magenta). The reconstructed energy matches the tritium beta spectrum well from 1 to 18 keV$_{\rm ee}$. The calibration data was acquired in a 40 hour time window in which less than three out of 115,000 events are expected to be non tritium [**?**],

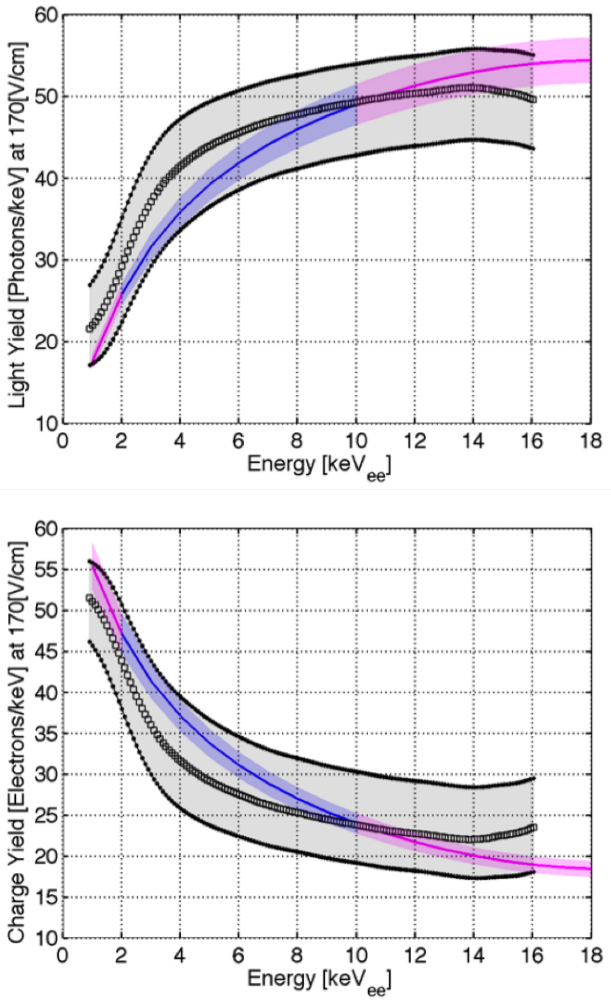

FIG. 8: The light yield and charge yield of ER events in LUX at 170 V/cm compared to NEST v0.98 (2013). The grey bands indicate the systematic errors on g_1 and g_2, which are fully correlated across all energy bins. g_1 is anti-correlated with g_2, such that an increase in the charge yield within the grey band must be compensated by an equivalent decrease in the light yield. Upper: Light yield at 170 V/cm. Lower: the charge yield at 170 V/cm.

this implies a near perfect data purity for the calibration. Nearly every point (99.997%) show in figure 13 and the histogram of 14 is the result of a tritium beta decay in the fiducial volume of the LUX detector.

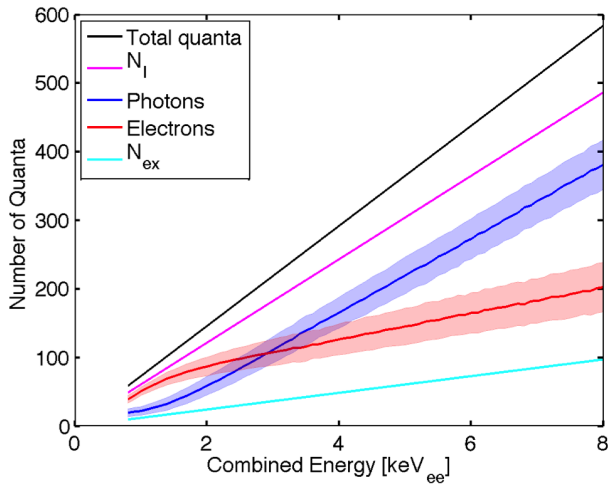

FIG. 9: The mean number of electrons (red) and scintillation photons (blue) produced in LUX at 170 V/cm as a function of energy. The bands indicate the correlated systematic errors on g_1 and g_2. Also shown are the total number of quanta, primary ions, and primary excitons, assuming an exciton to ion ratio of 0.2.

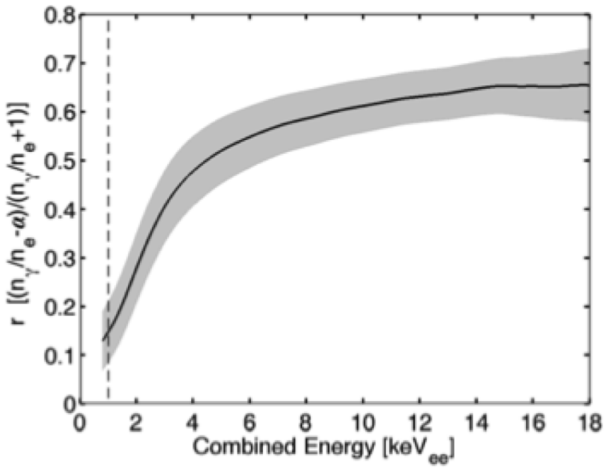

FIG. 10: Recombination fraction of ER events at 170 V/cm, assuming an exciton-to-ion ratio of 0.2.

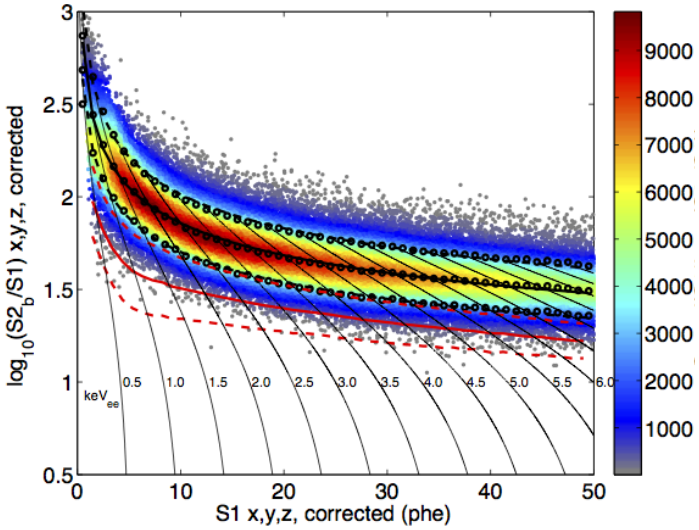

FIG. 11: The electron recoil band of LUX illuminated by 115,000 tritium events at the nominal LUX electric field of 170 V/cm. The recoil discriminant variable, log(S2/S1), is shown vs. S1 between 1 and 50 phe in S1 (about $1-8\mathrm{keV_{ee}}$). Also indicated in black are the mean and the 10% and 90% contours. The solid red line represents the mean NR band determined with NEST v0.98 (2013) [**?**] and validated with AmBe and ^{252}Cf neutron sources and the DD neutron generator data. The dashed red indicates the 10% and 90% contours of the NR band.

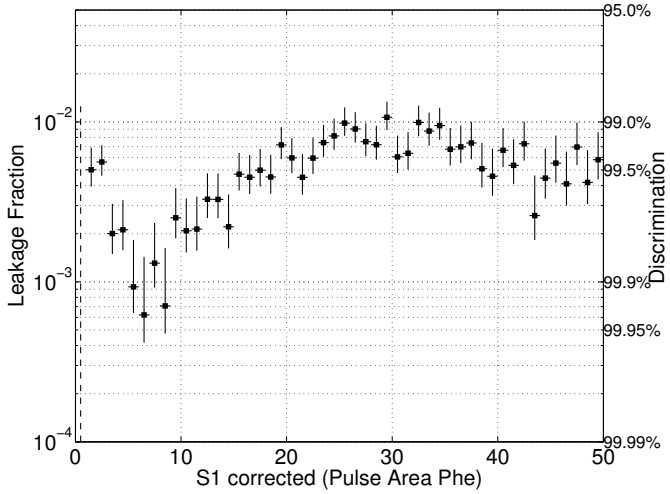

FIG. 12: LUX recoil discrimination vs. S1, determined from Fig. 11. Y-axis labels: left - leakage fraction (f); right - discrimination ($1-f$).

1. Threshold Determination

The tritiated methane calibration source provides beta decays with energies down to 0.1 $\mathrm{keV_{ee}}$ allowing for an independent measure the LUX detector's threshold. The limitation for detecting a single scatter WIMP like event event with PMTs is the S1 (primary scintillation) signal, being more than an order of magnitude less than the S2 signal. The S1 threshold could be measured by comparing the NEST model, assuming perfect detector resolution, to the observed tritium beta spectrum from 0.1-10 $\mathrm{keV_{ee}}$. The threshold determined by comparing the tritium data to NEST is in good agreement with all other methods used for determining the threshold in the LUX detector, figure 15.

IV. Additional Calibrations with Tritium

In this paper we have described the development and use of a tritiated methane calibration source for large scale xenon detectors. The primary application of the tritiated methane calibration source is to characterize the ER band and measure discrimination from electronic and nuclear recoils. However, much more fundamental xenon physics can be probed with the tritium calibration source. With higher statistics the discrimination can be measured in finer bins of energy or S1 Phe (figure 12) along with the Gaussianity of the ER band. The log(S2/S1) has been assumed to have Gaussian behavior in past experiments, never before has there been an ER calibration with such high data purity in the WIMP search region to observe potential non-Gaussian behavior. The largest tritium calibration in LUX detector's fiducial region produced 115,000 tritium beta decays with only three being non tritium events. The tritium calibration can also used to calculate the light yield, charge yield and recombination fluctuation over the range from 1 to 18 $\mathrm{KeV_{ee}}$. The current data taken with the LUX detector has allowed for the vetting of the NEST model down to 1 $\mathrm{keV_{ee}}$ for the first time. Finally, tritium provides a low energy uniformly distributed source making it ideal for determining the fiducial volume of a de-

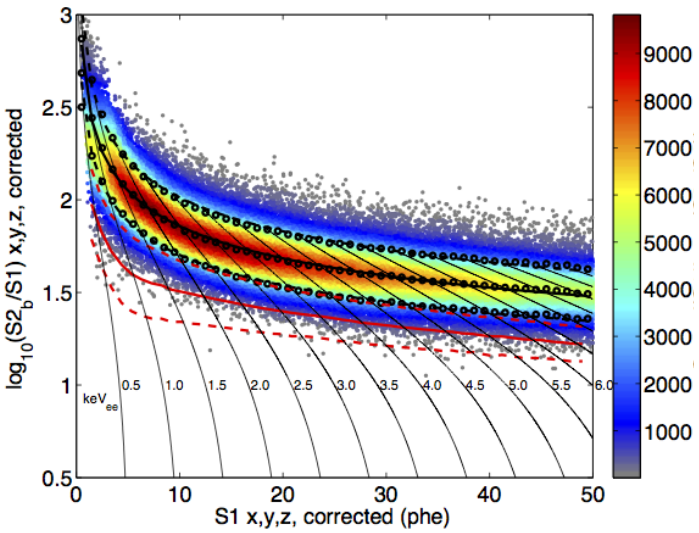

FIG. 13: Discrimination vs. S1 using over 115,000 tritium beta decays between 1 and 50 Phe in S1 (about $1-8\mathrm{keV_{ee}}$). On average from 1 to 30 Phe the discrimination is 99.58%, defined by the fraction of events of events below the mean of the nuclear recoil band. The red band represents the NEST nuclear recoil band (version 0.98) vetted with an AmBe, ^{252}Cf and DD neutron generator calibration.

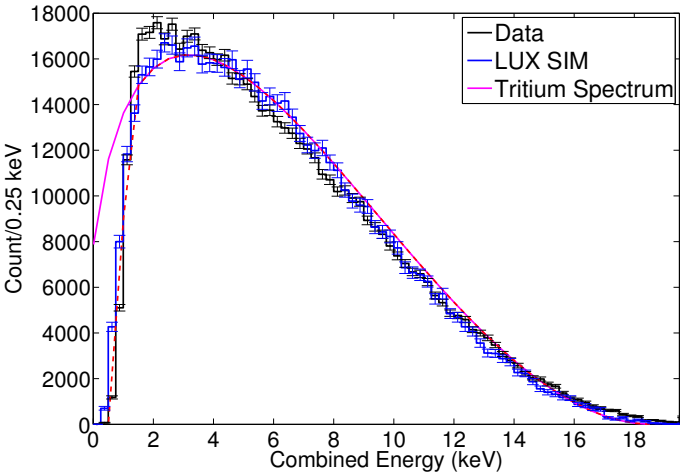

FIG. 14: Energy histogram of tritium events. The black histogram represents the data, in blue is the tritium spectrum produced with LUX SIM based on NEST. The magenta curve shows the true tritium beta spectrum without smearing due to finite detector resolution, the dashed line indicates the true tritium spectrum convolved with the threshold

tector and calibrating position reconstruction algorithms for low energy events.

V. Summary

We have presented our new technique for injecting and removing CH_3T as an internal calibration source in detectors which utilize liquid and gas phase noble gases. We discussed the assembly of our CH_3T calibration system, motivated by gas and liquid phase R&D experiments at the University of Maryland. We have used data from the LUX detector to show that our system can safely inject CH_3T for the purpose of internal calibration.

1 Outgassing of Tritiated Methane from Plastics

An accurate model of a tritiated methane injection into LUX must account for outgassing of CH_3T from plastics such as polyethylene and teflon. Duhamel's priciple, an integral solution to Fick's second law on a half-infinite line is found to be

$$\phi(x,t) = KC_{out} - \int_0^t erf(\tfrac{x}{\sqrt{4D(t-\tau)}})KC_{out}^{\cdot}(\tau)d\tau - KC_{out}(0)erf(\tfrac{x}{\sqrt{4Dt}}),$$

where K is the solubility of the material, D is the diffusion constant, and C_{out} is the concentration at the surface of the material. For the outgassing process we are only able to detect the flux of material out of the plastic. This is given by Fick's first law evaluated at $x = 0$,

$$J_{out}(t) = -K\sqrt{\frac{D}{\pi}}\left(\int_0^t \frac{C_{out}^{\cdot}(\tau)}{\sqrt{t-\tau}}d\tau + \frac{C_{out}(t)}{\sqrt{t}}\right),$$

where the sign has been flipped since the flux of material is outward. It is no longer possible to evaluate K and

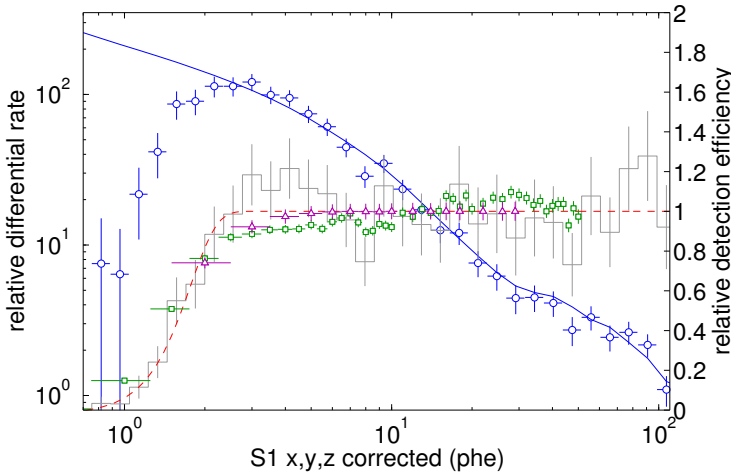

FIG. 15: Comparison of AmBe data (blue circles) with NEST simulations (blue line), showing excellent agreement above the 2 phe threshold (left axis). The gray histogram and fitted dashed red line show the relative efficiency for detection of nuclear recoils from AmBe data (right axis). Overlaid are the ER detection efficiency from tritium data (green squares), applied to the ER background model in the profile likelihood analysis, and the efficiency from full detector NR simulations treated as real data in terms of the digitized MC-truth S1 phe (purple triangles), applied to the WIMP signal model. The efficiency calculation here does not include S1 or S2 area thresholds.

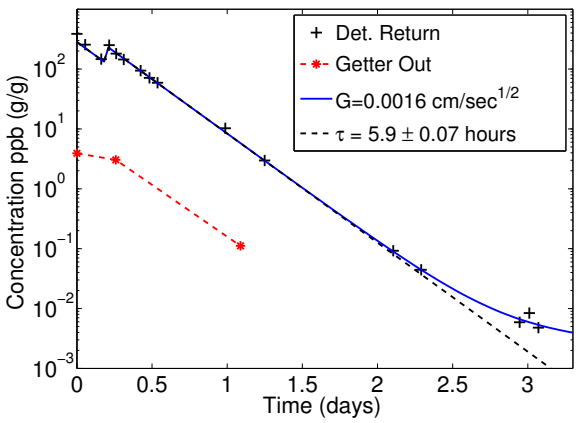

FIG. 16: Removal of natural methane observed by the integrated xenon sampling system prior to the tritiated methane injections. The red points indicate measurements at the getter outlet, we find a 97% one pass removal efficiency at a flow rate of 25 SLPM. The blue curve shows the upper limit on the effect of outgassing from the plastics. The black dashed lines shows the exponential fit to the natural methane removal from the xenon with a time constant of 5.9 ±0.07 hours. 5×10^{-3} ppb (g/g) is the limit of detection for methane.

D separately, since the diffusion in and out of the plastic is completely determined by the time-dependent concentration outside of the plastic. To simplify our model, we define a new constant

$$G = K\sqrt{\frac{D}{\pi}}.$$

Using data from the LUX sampling system we set an upper limit of $G < 0.0016 \frac{cm}{\sqrt{day}}$.

With a constraint on G taken from the analytic solution to Fick's second law, we turn to numerical simulation to answer the question of how much initial CH_3T activity to inject into LUX to meet our calibration goals. We set a limit of 0.33 μBq (5% of the LUX ER background rate design goal) from residual CH_3T activity after an injection. Several assumptions are made to simplify the numerical model. First, we approximate the diffusion into plastic as being a one dimensional process. Since the plastic in LUX can be approximated by a cylindrical shell there is no dependence on the azimuthal or z coordinates. Since r is large compared to the thickness of the plastic shell, $\frac{\delta^2\phi}{\delta r^2} \gg \frac{1}{r}\frac{\delta\phi}{\delta r}$, so Fick's laws in a one dimensional approximation become

$$J = -D\frac{\delta\phi}{\delta r}\vec{r}$$

$$\frac{\delta\phi}{\delta t} = D\frac{\delta^2\phi}{\delta r^2}.$$

We assume the concentration of CH_3T in LUX is uniform throughout its volume, since the design of LUX creates currents which stir the liquid xenon. With perfect mixing the effect of the purifier can be modeled by adding an exponential time dependence of 5.9 ±0.07 hours to the outer volume.

We use a simple implementation of the first order Euler method for to produce numerical simulations of the resid-

ual activity in LUX after a CH_3T injection. The diffusion is simulated by setting the concentration at the boundary of the piece equal to KC_{out}, where C_{out} is the concentration of CH_3T in the xenon. This concentration is dependent on time according to

$$\frac{\delta C_{out}}{\delta t} = J_{out}\frac{A_{plastic}}{V_{xenon}} - \frac{C_{out}}{\tau},$$

where $A_{plastic}$ is the surface area of the plastic cylinder, V_{xenon} is the total volume of xenon in the fiducial region, and τ is the characteristic removal time of methane from LUX. The first term on the right of this equation models outgassing of CH_3T from the plastic cylinder, while the second term models removal of CH_3T through purification. Using the first order Euler method, we arrive at an expression for C_{out} given by

$$C_{j+1} = C_j + \Delta t\left[(J_{1,j} - J_{N_x,j})\frac{A_{plastic}}{V_{xenon}} - \frac{C_j}{\tau}\right].$$

The initial concentration is defined by dividing the desired injection activity by the volume of the fiducial region. We choose $D = 2.3\times10^{-9}\frac{cm^2}{sec}$ so that the half-infinite boundary conditions in our diffusion model is valid, and combine this with our upper limit on G to extract a value for K. We use this model to predict the total number of calibration events as well as the time required to return to <5% of the nominal background rate for any CH_3T injection into LUX.

Figure 19 shows the results of our simulations for a 1 Bq and 10 Bq injection into LUX. We find that for moderate injections on the order of 1 Bq we reach our limit of 0.33 μBq in ?? days after the initial injection. For larger injections it can take longer than ?? days to reach our background limit. While these simulations use a conservative upper limit for the value of G it emphasizes that injecting too much CH_3T into LUX can lead significant delays in a WIMP search.

2 Tritiated Methane Removal

The removal efficiency of zirconium getters for CH4 in xenon had previously been studied at the University of Maryland. It was found that greater than 99.99% of natural methane can be removed in a single pass through a zirconium getter. [**?**] Tritiated methane is chemically identical to natural methane, so it follows that similar removal efficiencies should be expected for CH_3T. To verify

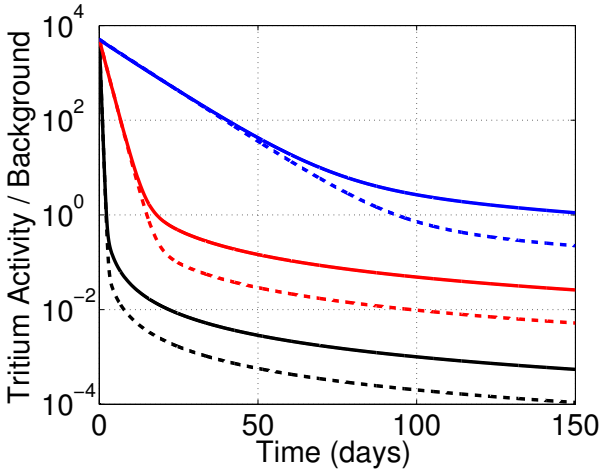

FIG. 17: Displayed are the results of simulated 0.1 Bq injections of tritiated methane into LUX. The dashed curves assume the lower limit of G (0.0015 cm/day$^{1/2}$, while the solid curves assume the upper limit of G (0.0075 cm/day$^{1/2}$). The black curves assume a characteristic removal time of 0.25 days, the black curves assume 1.7 days, and the blue curves assume 10 days.

this a small scale tritiated methane injection system was integrated into a liquid xenon system at the University of Maryland. This system used a SAES MC1-905F methane purifier placed in series immediately after the CH_3T source bottle to prevent non-methane species of tritium from entering the plumbing. Over 68,000 Bq of observed CH_3T activity was injected into this small scale system and a removal efficiency of over 99.99% for tritiated methane in xenon was confirmed.

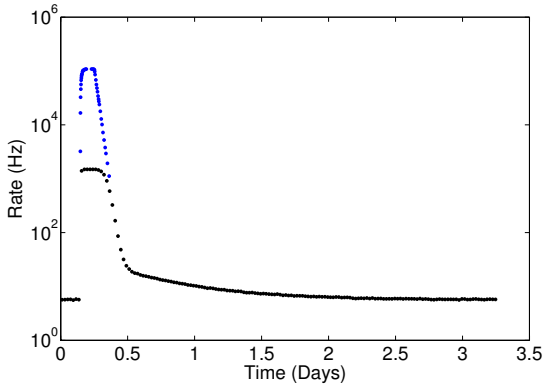

FIG. 18: A time histogram of the event rate during a tritium injection into our small scale detector. The event rate greatly exceeded the limits of our ADC (black data points), so a analog scalar was used to count the true event rate (blue data points).